A Simple Boundary Condition for Unbounded Hyperbolic Flows

I. ORLANSKI

Geophysical Fluid Dynamics Laboratory/NOAA, Princeton University,
Princeton, New Jersey 08540

A Sommerfeld radiation condition (2.2) is proposed for problems requiring a prescribed open boundary. The equations must be hyperbolic in nature (although the author believes that they may also be good for some elliptic and parabolic problems). It is proven that the proposed condition was shown to be free of reflection for single wave propagation. Two severe tests were used to demonstrate the applicability of the open boundary condition: (i) the collapsing bubble, a dynamic event which excites many different internal gravity waves. The results show minimum distortion. (ii) The spatially growing K–H instability. This test differs from the previous one in that the only waves excited are those corresponding to the maximum unstable wavelengths. In this case, the maximum amplitude is reached at the open boundary. As it has been shown, the open boundary condition (2.2) produces minimum distortion.

1. INTRODUCTION

The increasing interest in the numerical simulation of local mesoscale processes in the atmosphere as well as in the ocean presents a *nontrivial* difficulty in prescribing boundary conditions for the finite area of the numerical integration. This difficulty arises due to our lack of knowledge of the dynamical behavior of the environment in the region outside this area. Obviously this type of problem is not new in fluid dynamics. A few examples in which some kind of open boundary condition must be prescribed include flows over obstacles, mountain flows, wake instability flows, etc.

What is needed in flow problems dominated by advection and/or wave motion is an "open" boundary condition; that is, a boundary condition which allows phenomena generated in the domain of interest to pass through the boundary without undergoing significant distortion and without influencing the interior solution. The open boundary condition problem is also relevant to the nesting problem in which a fine mesh model is nested in a model with coarser mesh. If waves are generated in the fine mesh region and cannot be resolved in the coarse

251

grid area due to lack of resolution, then some kind of open boundary condition must be applied in the borders of the fine mesh region.

Obviously, since a physical law to prescribe the boundary condition in an open domain for any general problem does not exist, some kind of extrapolation must be used in order to obtain such boundary conditions. The appropriate type of extrapolation will depend largely upon the character of the equations to be solved (hyperbolic, elliptic, or parabolic). The equations of motion for the description of atmospheric dynamics could behave like any of the three types of equations mentioned above. Our interest in the present work is focused on mesoscale problems, wave propagation, and any disturbances that are generated in the domain of integration, and in time leave the systems; phenomena which are characterized by hyperbolic systems. A variety of methods have been developed to achieve open boundary conditions for such systems. Without describing the well-known periodic boundary condition, examples of the other boundary conditions are:

(i)   Sommerfeld radiation condition;

(ii) one-side differencing method;

(iii) Newtonian damping ("sponge") or viscous damping at the boundaries.

Condition (i) has been most widely used in theoretical studies because the dispersion characteristics of the waves needed to prescribe the Sommerfeld radiation condition are known as follows:

$$(\partial \phi / \partial t) + C\phi_x = 0, \tag{1.1}$$

where ϕ is any variable, and C is the phase velocity of the waves. The numerical equations for mesoscale processes are nonlinear and the dispersion characteristics are not generally known. One method used by Kreiss [1] for avoiding this problem assumes that the characteristics of the waves will have a slope equal to $\Delta x/\Delta t$ (Δx and Δt being the spatial and temporal gridsize, respectively). Then, the extrapolated variable ϕ at the present time step τ at the boundary point JM will be given by:

$$\phi^\tau(JM) = 2\phi^{\tau-1}(JM - 1) - \phi^{\tau-2}(JM - 2) \tag{1.2}$$

This relation is similar to the one obtained from Eq. (1.1), if $C = \Delta x/\Delta t$ or that the phase velocity, C, is equal to the maximum feasible numerical velocity $\Delta x/\Delta t$; since the finite leap-frog difference representation of Eq. (1.1) is:

$$\frac{\phi^\tau(JM) - \phi^{\tau-2}(JM)}{2\,\Delta t} = -\frac{C}{\Delta x}\left[\frac{\phi^\tau(JM) + \phi^{\tau-2}}{2}(JM) - \phi^{\tau-1}(JM - 1)\right],^1 \tag{1.3}$$

---

[1] The form used in Eq. (1.3) to express ϕ_x is such that it involves only points of the same numerical mode, since it is known that such schemes such as leap-frog can produce an artificial modal splitting. In such cases, the boundary condition mixes these modes in a different way than the interior equation, then strong reflection can occur.

where, in particular, if $C = \Delta x/\Delta t$, then Eq. (1.3) becomes:

$$\phi^\tau(JM) = \phi^{\tau-1}(JM - 1). \tag{1.4}$$

The previous boundary conditions (1.2) or (1.4), performs reasonably well when the numerical solution is characterized by one single wave with phase velocity approximating $\Delta x/\Delta t$. However, if this is not the case, reflection will occur at the boundaries. A modification of the Kreiss method was shown by Pearson [2] and others in which C is estimated from the linearized dispersion relation, taking C to be the phase velocity to the dominant wave. Again, this method depends on knowing a dispersion relation that, as a rule, is not known in complicated geophysical flows.

The one-side differencing methods (ii) will not be described in detail here since they were very much in use in the early 1960's. They were used with some success in problems involving strong advection and smooth disturbances at the boundary; however, with large disturbances, reflection and instabilities developed very quickly.

In group (iii) viscous damping has been used with some success in mesoscale modeling by Bushby and Timpson [3]. However, the large variation of viscosity at the boundary produces some reflections and the method wastes a significant number of gridpoints close to the boundary. Quite recently, Piacsek (personal communication, Lindman [4]), has developed a method that uses Newtonian damping to force the solution to some known boundary condition.) The disadvantage here is that for the damping to be gradual, several gridpoints are wasted. Also, waves traveling tangential to the boundary may be distorted by spatial variation of damping. In the next section, a simple boundary condition will be formulated that has been shown to be efficient in minimizing reflection in quite dissimilar situations. A demonstration of the effectiveness of the boundary condition in several flow problems is given in Sections 4 and 5, with a description of the model used given in Section 3.

2. OPEN BOUNDARY CONDITIONS

The suggested approach to be employed here involves use of the Sommerfeld radiation condition (Eq. (1.3)) at the boundary; but in a form different from that previously discussed by Kreiss and Pearson, among others. Instead of fixing a constant value for the phase velocity, we numerically calculate a propagation velocity from the neighboring grid points, using the same Eq. (1.3) for each variable to calculate C.

$$C_\phi = - \frac{[\phi^\tau(JM - 1) - \phi^{\tau-2}(JM - 1)]}{[\phi^\tau(JM - 1) + \phi^{\tau-2}(JM - 1) - \phi^{\tau-1}(JM - 2)]} \frac{\Delta x}{2\,\Delta t}, \tag{2.1}$$

and then to determine the boundary gridpoint the following relation is used:

$$\phi^{\tau+1}(JM) = \frac{[1 - (\varDelta t/\varDelta x)\, C_\phi]}{[1 + (\varDelta t/\varDelta x)\, C_\phi]} \,\phi^{\tau-1}(JM) + \frac{2(\varDelta t/\varDelta x)\, C_\phi}{[1 + (\varDelta t/\varDelta x)\, C_\phi]} \,\phi^{\tau}(JM - 1). \quad (2.2)$$

In this formulation, we require that $0 \leqslant C < \varDelta x/\varDelta t$. Then, for the limiting outflow condition, $C_\phi = \varDelta x/\varDelta t$, Eq. (2.2) gives

$$\phi^{\tau+1}(JM) = \phi^{\tau}(JM - 1), \quad (2.3)$$

which is similar to the condition (1.2) for pure waves. Conversely, in the limit $C_\phi = 0$, then

$$\phi^{\tau+1}(JM) = \text{either} \quad \phi^{\tau-1}(JM)$$
$$= \text{or} \quad \phi \text{ boundary.} \quad (2.4)$$

No information has come from the interior solution, so we must regard this as inflow information, to be prescribed from a previous time step or as a boundary.

It should be pointed out that since each atmospheric variable ϕ is determined by a different equation, the numerical propagation velocities C_ϕ can be different from each other and must be computed separately. Also the expressions (2.3) and (2.4) shows the limiting values that will take any velocity. The final form for each of these velocities will then be:

$$C_\phi = \varDelta x/\varDelta t, \quad \text{if } -\phi_t/\phi_x > \varDelta x/\varDelta t,$$
$$C_\phi = -\phi_t/\phi_x, \quad \text{if } 0 < -\phi_t/\phi_x < \varDelta x/\varDelta t; \quad (2.5)$$
$$C_\phi = 0, \quad \text{if } -\phi_t/\phi_x < 0.$$

Note that this boundary condition does not depend upon global quantities, such as mean flow properties, for the purpose of determining whether inflow or outflow exists at a given point on the boundary. The condition should thusly prove to be very useful for cases in which a weak mean flow is present and an initial inflow boundary condition could be changed to an outflow condition due to the presence of upstream propagating waves in the domain of integration.

The boundary condition (2.2) is nonlinear in nature. Therefore, a theoretical analysis of its reflection characteristics is not possible for the general case. We will demonstrate the nonlinear behavior of the boundary condition by using it in several numerical solutions in Sections 4 and 5. However, for the present, we will prove that a single wave will not be reflected by this boundary condition.

Using (2.1) and (2.2), we obtain

$$\phi^{\tau+1}(JM) = \frac{\phi^{\tau}(JM-1) - \phi^{\tau-1}(JM-2)\ \phi^{\tau-1}(JM)}{\phi^{\tau-2}(JM-1) - \phi^{\tau-1}(JM-2)}$$

$$- \frac{\phi^{\tau}(JM-1) - \phi^{\tau-2}(JM-1)}{\phi^{\tau-2}(JM-1) - \phi^{\tau-1}(JM-2)}\ \phi^{\tau}(JM-1). \quad (2.6)$$

It should be noted that if $\phi^{\tau}(JM-1) = \phi^{\tau-1}(JM-2)$, then $\phi^{\tau+1}(JM) = \phi^{\tau}$ $(JM-1)$, this is the limiting case in which the phase speed is precisely $C_\phi = \Delta x / \Delta t$.

To see that the boundary condition (2.6) gives no reflection for a single wave component, it is sufficient to substitute into it the wave:

$$\phi^{\tau}(J) = \phi_0 \exp(i(KJ\Delta x - \omega t \Delta t)), \quad (2.7)$$

which satisfies (2.6) in an identical fashion. This is not surprising, since the wave (2.7) has a constant phase speed, which the scheme measures at time $\tau - 1$ and then applies at time τ. Until now, only the one-dimensional problem has been discussed. However, the same condition applies for two- and three-dimensional problems. The extrapolation (2.2) is valid in so far as the propagation speed C_ϕ in (2.7) is taken to be the normal component to the open boundary. Suppose that ϕ is expressed as a three-dimensional wave

$$\phi = \phi_0 \exp(i(kx + ly + \gamma z - \omega t)), \quad (2.8)$$

where k, l, and γ are the three components of the wavenumber vector. $k = k\mathbf{i} + l\mathbf{j} + \gamma\mathbf{p}$. In this case any of the following three relations is valid:

$$(\partial\phi/\partial t) + C^i(\partial\phi/\partial_{x_i}) = 0. \quad (2.9)$$

Note that the product $C^i(\partial/\partial x_i)$ is not an indication of summation but of the individual product in the normal direction to the boundary where $C^i = (\omega/\mathbf{k}_i)$ and $\mathbf{k}_i$ is the component of the wavenumber in the X_i direction. The relation (2.9) is, of course, the Sommerfeld radiation condition (1.1) from which the extrapolation (2.2) was derived. We must conclude then that this extrapolation is generally true for any dimensions.

3. Model Description

The numerical model described below has been designed to simulate the behavior of a two-dimensional stratified fluid in a rectangular container. In the examples treated in this paper, the container has a rectangular cross section with width L

and height H, and is filled with a stratified fluid (linear in the collapsing bubble experiment and with a hyperbolic tangent profile for the Kelvin–Helmholtz instability). The fluid is incompressible with the Boussinesq approximation assumed.

The condition of two-dimensionality allows us to formulate the Navier–Stokes equations in terms of stream function ψ and vorticity ζ. The resulting equations may be written as follows:

$$\partial \zeta / \partial t = J(\psi, \zeta) + (\partial \theta / \partial x) + \nabla \nu \nabla \zeta, \tag{3.1}$$

$$\partial \theta / \partial t = J(\psi, \theta) + \nabla \kappa \nabla \theta, \tag{3.2}$$

$$\nabla^2 \psi = \zeta, \tag{3.3}$$

where θ is the potential temperature, and ν and κ are the eddy viscosity and diffusivity respectively, as defined in Orlanski and Ross [5].

The finite-difference formulation of the above equations is identical to the scheme used by Orlanski and Ross except for the method of solution of the Poisson equation (3.3). This method of solution is a simple ADI technique similar to that described by Peaceman and Rachford [6]. The gridnet is made up of 51 gridpoints in the vertical, and 42 or 66 gridpoints in the horizontal.

The boundary conditions used on the rigid top ($Z = H$) and bottom ($Z = 0$) are:

$$\psi = \zeta = 0 \quad \text{and} \quad \theta_z = \bar{\theta}_z, \tag{3.4}$$

where $\bar{\theta}_z$ is the local initial lapse rate for temperature.

We apply the open boundary condition (2.2) described in the previous section to the left and right boundaries, noting that the propagation velocities C_θ and C_ζ were calculated from Eq. (2.5) for temperature and vorticity. The value for stream function at the boundary is calculated from the same relation (2.2) but with the vorticity propagation velocity C_ζ used.

Further details regarding boundary condition treatment will be given in the succeeding sections in which the modeling of specific experiments will be described.

4. COLLAPSE OF A MIXED REGION IN A STRATIFIED FLUID

In this section we will discuss the simulation of the collapse of a two-dimensional mixed region immersed in a stratified fluid, this is typical of a homogeneous density bubble immersed in a fluid, density of which varies linearly with height (Young and Hirt [7]). Such a simulation provides us with an opportunity to compare solutions from our numerical model for two different container lengths;

41 Δx and 65 Δx, with open boundary conditions in each case. The ideal situation would be for the solution of the smaller region to exactly match the corresponding solution of the larger region in the region common to both. Figure 1 shows the initial temperature fields for the larger and smaller domains with dashed lines in the upper part of the figure enclosing the region common to both solutions. Most of the remaining figures are arranged in the same manner as Fig. 1. The figures in this section are divided into two groups: *New Extrapolation* (NE) (referring to use of the new boundary condition proposed in (2.2)) and *Simple Extrapolation* (SE) (for use of the simple outflow scheme (2.3)).
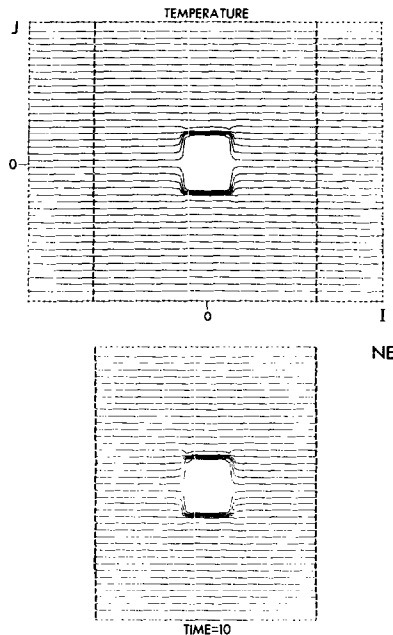
FIG. 1. Contours of temperature using the new extrapolation (NE) at 10 time steps. The zeroes mark the midpoint in the horizontal (I) and the vertical (J) directions. The temperature field in the upper half of the figure is $65\Delta x$ in the horizontal; the lower one is $41\Delta x$ in the horizontal and both are $50\Delta z$ in the vertical. The dashed lines show the area which is common to both fields.

The horizontal velocity U after ten time steps is shown in Fig. 2. The symmetrical maximum velocity to the left and right of the mixed region indicates that the initial tendency of the bubble is to collapse sideways. This abrupt change in the temperature (density) pattern produces gravity waves which propagate outwards from the region of collapse.
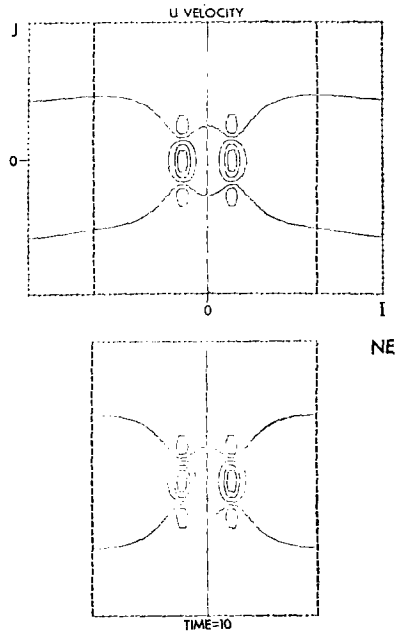
FIG. 2.   Similar to Fig. 1 but for U velocity.

Figures 3 and 4 show the corresponding horizontal U velocity for 150 time steps, as waves and the collapsed region tend to spread out of the center regions. A simple outflow boundary condition at the boundaries is expected to perform well in a numerical simulation as shown in Fig. 4.

At approximately 300 time steps, the maximum disturbances reach the open boundaries in the smaller domain. Some differences can be noticed in the temperature field. However, the discrepancies are apparent in the U velocity field in Fig. 5, but quite obvious in the simple extrapolation in Fig. 6. The differences between the smaller and larger domains seen in Fig. 5 are not substantial and mainly affect the higher wavenumbers due to partial reflection at the boundaries. These high wave numbers are present because no appreciable damping was applied in this numerical simulation. In Fig. 6, the larger discrepancies between two solutions in the simple extrapolation case are generated because of the intensification of the reflection of small scale disturbances, since this particular extrapolation implies a constant phase velocity equal to $\Delta x/\Delta t$. Then waves with smaller phase velocity will be reflected.

The comparisons between the history records for the time fluctuation of temperature are shown in Fig. 7 for NE and in Fig. 8 for SE. These were taken at a distance of $L/4$ from the left boundary and $H/10$ from the center line. Notice that the phase
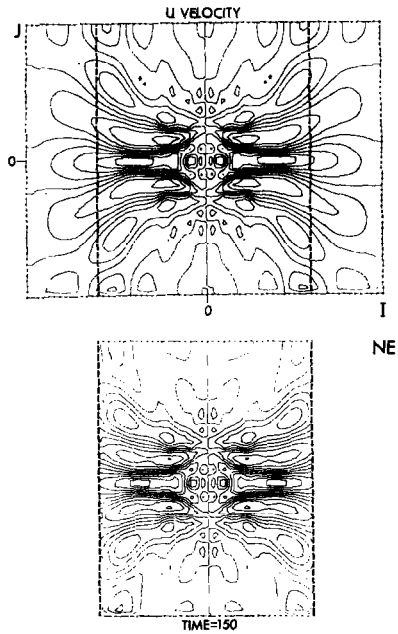
U VELOCITY

FIG. 3. As in Fig. 2 but contours of U velocity at 150 time steps.
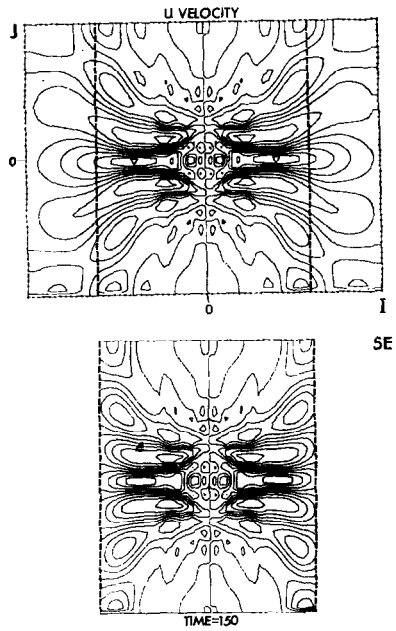
U VELOCITY

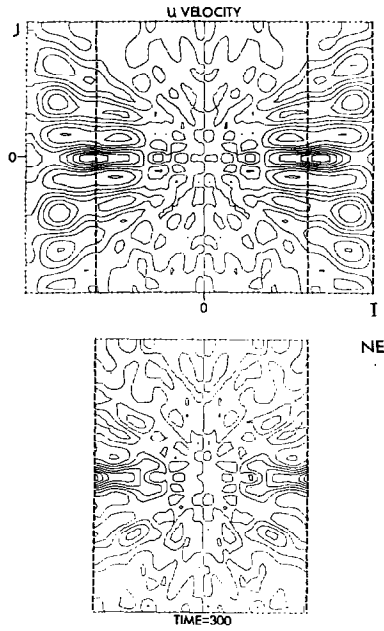FIG. 4. As in Fig. 3 but for the simple extrapolation case.

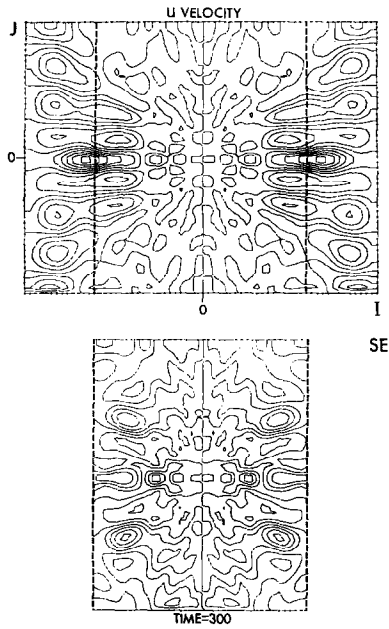FIG. 5. *U* velocity contours as in Fig. 2 at 300 time steps.

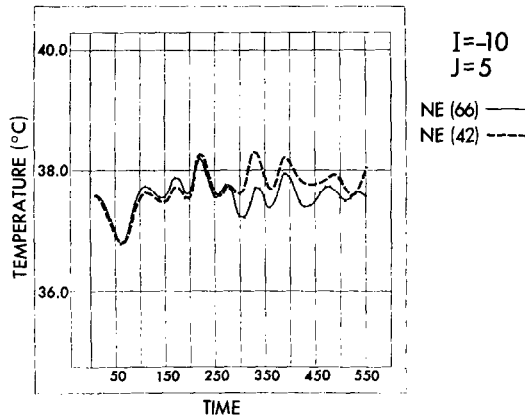FIG. 6. As in Fig. 9 but for the simple extrapolation case.

FIG. 7.   A comparison of history records of time variation of temperature between the new extrapolation 66 and 42 cases. The history checkpoint is at $I = -10$ and $J = 5$.
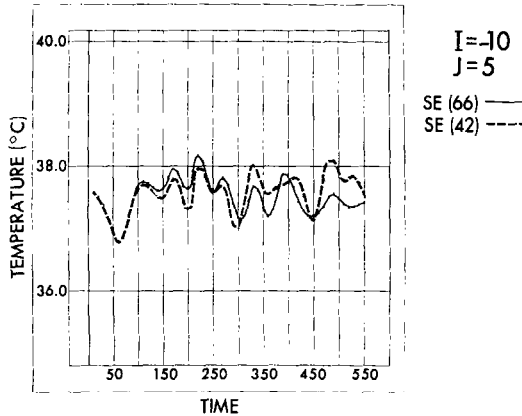

FIG. 8.   The same as Fig. 11 but for the simple extrapolation case.

of the disturbance is well simulated in both cases, but that the amplitudes begin to diverge toward the end of the record. One possible explanation of such behavior is that, in this particular experiment, the main dynamic region, (the collapsing bubble) is expelled from the interior domain through the boundaries by its own vorticity, implying that the advection field is moving with the source that generated it. Then when the bubble reaches the boundary and attempts to pass through, it will do so, but with a inevitable change in its advected velocity. This effect does not appear to produce considerable reflections.

It is of interest to compare equivalent solutions with the open boundary condi-

tions NE and SE, and the solution that will be obtained if simple reflecting walls are used. Figure 9 shows three different solutions of the collapsing bubble at 800 time steps. (Note that this experiment is slightly different in geometry than the previous one. In this case, only the right half of the domain is calculated with a symmetry boundary condition used on the left boundary.) Figure 9(a) shows the temperature disturbance solution for the case with a rigid wall condition applied to the right boundary. Figure 9(b) exhibits the same field for the case of the simple boundary conditions SE, and Fig. 9(c) shows the field for the solution with the new boundary
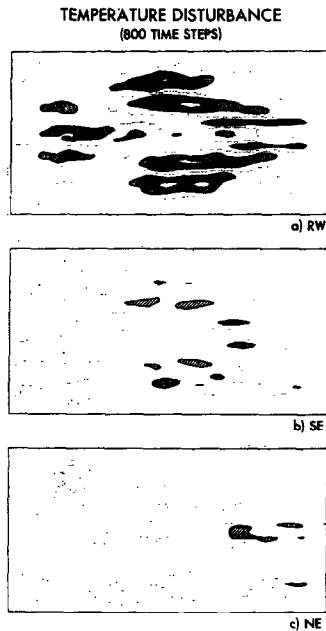

FIG. 9. Temperature disturbance at 800 time steps for different boundary conditions (a) rigid wall, (b) SE, (c) NE.

condition NE. Comparison of these three solutions shows that NE produces a solution with the least disturbances inside the domain of integration, thereby implying that the open boundary condition NE allows energy to leave the domain with a minimum amount of reflection.

In the previously discussed experiments in which both the left and right boundary conditions were of the "outflow" type over the total length of the integration, both the SE and NE seem adequate to be used as boundary conditions. It is possible that the NE is slightly better than the SE, but the application of the former is con-

siderably more complicated. In this regard, we may then conclude that if outflow conditions are warranted at all times, the use of NE or SE will be equally satisfactory. However, outflow conditions for the entire integration are very difficult to dictate in a stratified fluid with a prescribed mean flow, unless the magnitude of the mean flow is always larger than the faster propagating waves generated inside the fluid. Usually this is not the case in geophysical problems, such as in the atmosphere or in the ocean, where the fluid may be subcritical at one time and supercritical at another time. At this point, waves which propagate downstream at one time may also propagate upstream the next time. Then the prescribed mean flow does not usually warrant outflow or inflow conditions which must be satisfied at all times. Under such conditions, NE since it calculates the local phase velocity and adjusts the inflow or outflow condition depending on the sign of the phase velocity, is expected to perform better than would a fixed extrapolation such as SE or a fixed condition that assumes inflow at all times.

To illustrate these points, two basic experiments (a) and (b) were performed with the same initial conditions of the previous experiments: the collapsing bubble. The only difference is the inclusion of a constant mean flow with direction positive to the right (a) weak mean flow, $\bar{u} = (1/240)(\varDelta x/\varDelta t)$, and (b) strong mean flow $\bar{u} = (1/4)(\varDelta x/\varDelta t)$. We compare the performance of NE with: case (a) SE on the right boundary (outflow), and case (b) SE in the right and left boundaries.

The results are displayed in Fig. 10, which shows the vorticity squared integrated along the last five points close to each boundary

$$\bar{\zeta}^2 = \sum_{J=1}^{JM} \sum_{I=1}^{5} \zeta^2(I, J)$$

as a function of time. The results for case (a) are displayed on the left of Fig. 10, and case (b) on the right.

First, case (a) will be explained. The solution NE shows a slight asymmetry from the left and right boundary which is obviously due to the small advective effect of the mean flow. However, the left and right boundary have a completely different behavior pattern for SE, since in this particular case the left boundary (inflow) variables were kept constantly equal to the initial values. The waves that propagate upstream are accumulated at this boundary, explaining the growth of the squared vorticity in this case. In the case of the strong mean flow, the NE solution still performs very well. As can be seen on the right of Fig. 10, the asymmetry between left and right boundary values of the vorticity squared is increased in comparison with case (a), this being due to the greater advective effect. In this last case, the SE solution (similar extrapolation in both right and left boundaries) shows that where there are strong outflow conditions (right boundary) the SE boundary condition performs very well but obviously behaves very poorly in the inflow condition at the left boundary.
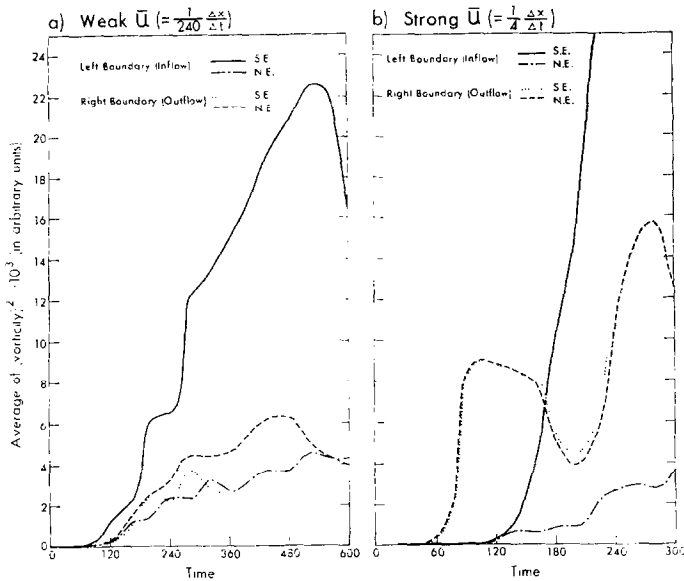
FIG. 10. (a) The integrated squared vorticity for left and right boundaries as a function of time for a weak mean flow in (a) similar for (b) but for the strong mean flow (see text).

From these previous results, we can conclude that for permanent outflow conditions, SE or NE are equally good. However, NE is far superior when the nature of the boundary condition changes in time, that being the more general case for open boundary conditions.

In the next section, we will discuss the performance of NE when spatially growing waves are considered. As an example, we chose the Kelvin–Helmholtz instability.

5. KELVIN–HELMHOLTZ INSTABILITY IN AN UNBOUNDED SHEAR FLOW

A considerable amount of observational data in the atmosphere and in the ocean relates to Kelvin–Helmholtz (K–H) waves and their generation of turbulence. One of the most common assumptions in analytic and numerical studies of the K–H instability involves the use of periodic boundary conditions and the resulting need to relate the temporal growth of the periodic wave to the spatial growth at an actual unbounded K–H wave. The amplitude of the waves at the outflow boundary will be at a maximum, producing large disturbances at the extrapolated values. Most of the boundary condition schemes used previously were incapable of reproducing good results or were limited to small amplitude waves.

Here, we will demonstrate that the proposed scheme (2.2) can be used in these extreme conditions. A few different initial conditions have been studied; the results of which will be reported elsewhere. In this section, we will show one simple experiment to illustrate the use of the boundary condition given by Eq. (2.2). The initial temperature field T and x velocity U are prescribed as

$$T = 15°\text{C} + 1°\text{C} \tanh(z/750 \text{ m}), \tag{5.1}$$

$$U = 40 \text{ m/sec} + 20 \text{ m/sec} \tanh(z/750 \text{ } m). \tag{5.2}$$

The minimum Richardson number that occurs in the center of the channel is 0.07; the height of the channel is 10^4 m, with 51 points evenly spaced in the vertical, and the two horizontal lengths used are 41 Δx and 65 Δx, with $\Delta x = 1000$ m. The time interval, Δt, is 5 sec. The inflow boundary is located at the left side. Note that the inflow condition of Eq. (2.2) will always set the current value (ϕ^τ) of the extra-polated variable to the value at $\phi^{\tau-2}$. This implies that if nondisturbances reach the left boundary from the interior, the inflow boundary will always retain the initial conditions.

If one wants to prescribe some inflow boundary conditions, it is necessary only to replace $\phi^{\tau-2}$ by the prescribed value. In the present case, we prescribe a small perturbation of stream function at the inflow boundary in order to excite the unstable waves. Another method which was used to disturb the solution over the entire domain with a random noise every 20 time steps. Since no significant differences could be found between these two methods (regarding the solution behavior at the open boundaries), we will discuss here only the solution with wave-like perturbation at the inflow boundary.

The perturbation forcing at the boundary is cyclic with a period of 200 sec (close to the period predicted by the linear K–H theory). After 100 time steps (500 sec), a well-formed wave can be seen in the vertical velocity fields of Fig. 11. As before, the upper field corresponds to $L = 65\Delta x$ and the lower to $L = 41\Delta x$. The waves propagate from left to right. The effect of the forcing extends only a few points away from the left boundary. In the interior region, the upper and lower solutions agree very well. The maximum unstable wavelength corresponds to $\lambda \simeq 11.400$ km. It is interesting to note from these figures (and from the others to be shown) that the most unstable wavelength changes spatially from a slightly shorter value close to the left boundary, to the value mentioned above at the right boundary. The reason for this can be easily seen. The forcing that we prescribe does not exactly correspond to the period of the most unstable wave. Of course, waves with the same period and forcing are also unstable and will be excited in the vicinity of the boundary forcing. However, downstream of this forcing region, the most unstable K–H wave will grow until it dominates the forced mode.

At the 200th time step (1000 sec), the amplitude of the wave at the right boundary
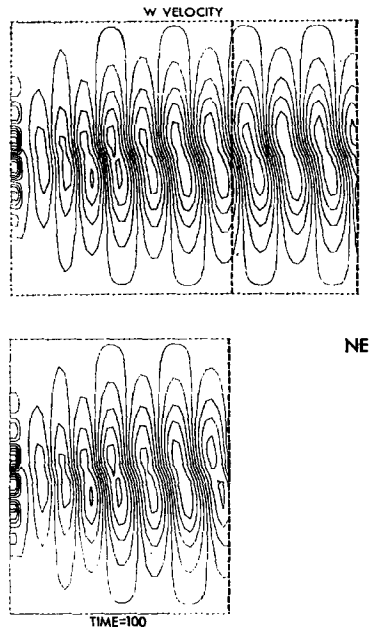
FIG. 11.   Contours of *W* velocity at 100 time steps in the Kelvin–Helmholtz case using the new extrapolation. The format is basically similar to that of Fig. 1 except that the area common to both fields now begins at the left boundary.

will grow at least 10 times the value at 100 time steps. Figure 12 shows the contours of vertical velocity (the contour intervals being different from Fig. 12 to Fig. 11). At this point, the spatial growing behavior of the waves is more evident. The contours of total temperature for this time in Fig. 13 show the patterns of the upper and lower solutions to be quite similar. The closed contours seen in the upper figure are not of signficant meaning since the solution in the region where they occur is practically flat and any small disturbances will create this observed pattern.

The next figure (Fig. 14) shows the temperature contours at 250 time steps (1250 sec). The upper figure effectively shows the spatial wave growth and the tendency for the wave to roll as seen in observational and experimental studies (Metcalf and Atlas [8], Delisi and Corcos [9], etc.) Even at this stage of a fully developed wave, it seems that the open boundary condition (2.2) in the smaller region $L = 41\Delta x$ permits a very accurate simulation of the K–H process.

In Fig. 15, a plot of temperature amplitude as a function of time is shown for both large and small domains at some point near the outflow boundary of the $L = 41\Delta x$ case. Again the agreement is remarkably good.
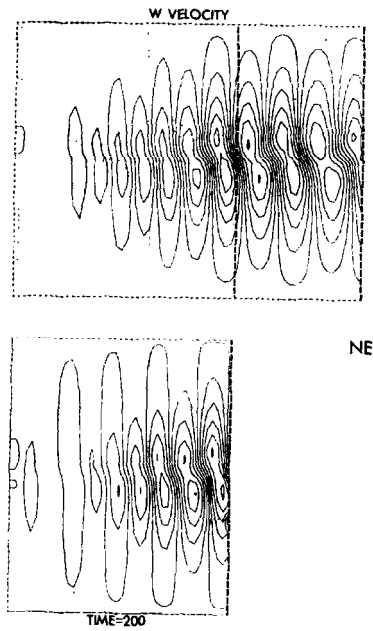
W VELOCITY

NE

TIME=200

FIG. 12.   As in Fig. 11, but at 200 time steps.

TEMPEPATURE

NE

TIME=200
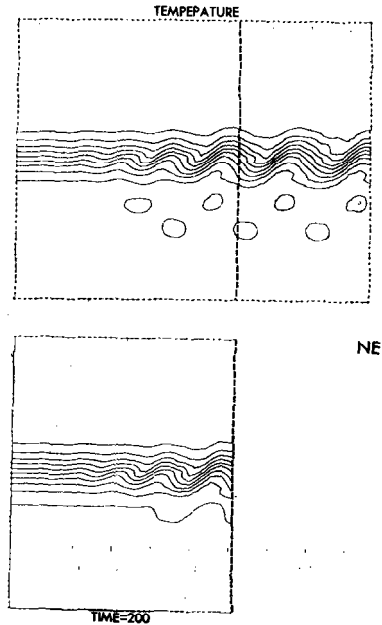
FIG. 13.   As in Fig. 12, but for temperature.
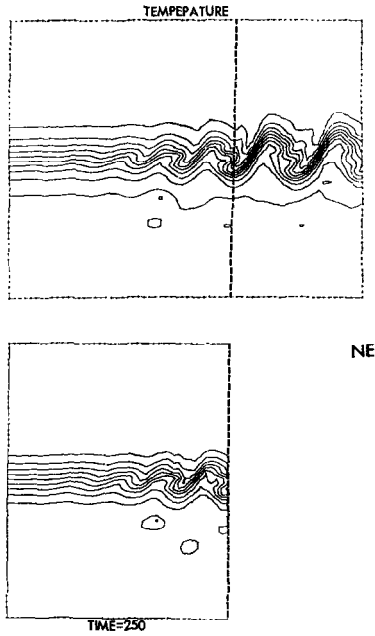
TEMPEPATURE

NE

TIME=250

FIG. 14. As in Fig. 13, but at 250 time steps.
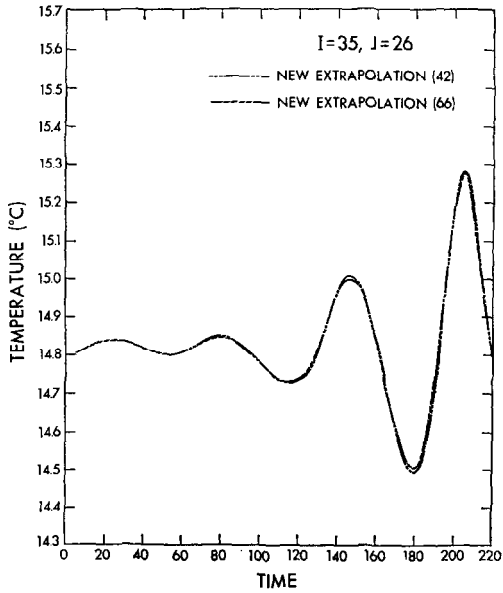

FIG. 15. A comparison of history records in the K-H case for the time variation of temperature. The history checkpoint is at $I = 35$ and $J = 26$.

6. CONCLUSION

A Sommerfeld radiation condition (2.2) in which a numerical evaluation of a phase velocity is performed in the vicinity of the boundary and extrapolated to that point is proposed for problems requiring a prescribed open boundary. The equations must be hyperbolic in nature (although the author believes that they may also be good for some elliptic and parabolic problems).

It was proven that the proposed condition was free of reflection for single wave propagation.

Two severe tests were used to demonstrate the applicability of the open boundary condition:

(i) The collapsing bubble, a dynamic event which excites many different internal gravity waves. The results show minimum distortion.

(ii) The spatially growing K–H instability. This test differs from the previous one in that the only waves excited are those corresponding to the maximum unstable wavelengths. In this case, the maximum amplitude is reached at the open boundary as has been shown, and the open boundary condition (2.2) behaves very well.

REFERENCES

1. H.-O. KREISS, "Proceedings of a Symposium at the University of Wisconsin," May, 1966), (Donald Greenspan, Ed.), Wiley, New York, 1966.
2. R. A. PEARSON, *J. Atmos. Sci.*, **31** (1974), 1481.
3. F. H. BUSHBY AND M. S. TIMPSON, *Quart. J. Roy. Meteor. Soc.* **93** (1967), 1.
4. LINDMAN, Sixth Conference on Numerical Simulation of Plasma, pp. 42–45. 1973.
5. I. ORLANSKI AND B. B. ROSS, *J. Geophys. Res.* **78** (1973), 8808.
6. D. W. PEACEMAN AND H. H. RACHFORD, *J. Soc. Indust. Appl. Math.* **3** (1955), 28.
7. J. YOUNG AND C. W. HIRT, *J. Fluid Mech.* **56** (1972), 265.
8. J. I. METCALF AND D. ATLAS, *Boundary Layer Meteorol.* **4** (1973), 7.
9. D. P. DELISI AND G. CORCOS, *Boundary Layer Meteorol.* **5** (1973), 121.